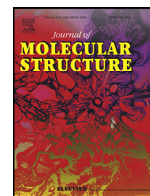




Since January 2020 Elsevier has created a COVID-19 resource centre with free information in English and Mandarin on the novel coronavirus COVID-19. The COVID-19 resource centre is hosted on Elsevier Connect, the company's public news and information website.

Elsevier hereby grants permission to make all its COVID-19-related research that is available on the COVID-19 resource centre - including this research content - immediately available in PubMed Central and other publicly funded repositories, such as the WHO COVID database with rights for unrestricted research re-use and analyses in any form or by any means with acknowledgement of the original source. These permissions are granted for free by Elsevier for as long as the COVID-19 resource centre remains active.



# In search of SARS CoV-2 replication inhibitors: Virtual screening, molecular dynamics simulations and ADMET analysis

Prinsa R. Nagar<sup>1</sup>, Normi D. Gajjar<sup>1</sup>, Tejas M. Dhameliya\*

L. M. College of Pharmacy, Navrangpura, Ahmedabad, Gujarat 380009, India

## ARTICLE INFO

### Article history:

Received 13 May 2021

Revised 11 July 2021

Accepted 24 July 2021

Available online 26 July 2021

### Keywords:

COVID-19

SARS CoV-2

Molecular docking

MD simulations

RdRp

ADMET assay

## ABSTRACT

Severe acute respiratory syndrome has relapsed recently as novel coronavirus causing a life threat to the entire world in the absence of an effective therapy. To hamper the replication of the deadly SARS CoV-2 inside the host cells, systematic *in silico* virtual screening of total 267,324 ligands from Asinex EliteSyn-ergy and BioDesign libraries has been performed using AutoDock Vina against RdRp. The molecular modeling studies revealed the identification of twenty-one macrocyclic hits (2–22) with better binding energy than remdesivir (1), marketed SARS CoV-2 inhibitor. Further, the analysis using rules for drug-likeness and their ADMET profile revealed the candidature of these hits due to superior oral bioavailability and druggability. Further, the MD simulation studies of top two hits (2 and 3) performed using GROMACS 2020.1 for 10 ns revealed their stability into the docked complexes. These results provide an important breakthrough in the design of macrocyclic hits as SARS CoV-2 RNA replicase inhibitor.

© 2021 Elsevier B.V. All rights reserved.

## 1. Introduction

Novel coronavirus (CoV) has been recognized as a deadly respiratory pathogen and causative agent for severe acute respiratory syndrome coronavirus-2 (SARS CoV-2) or coronavirus disease 2019 (COVID-19) [1] since its outbreak in the Hubei province of Wuhan, China in 2019 [2,3]. It has caused an unprecedented pandemic worldwide with the higher fatality rate than the previously known SARS CoV. The background of the virus traces back nearly two decades to a closely related previously emerged pathogen having genomic similarity of 75–80% [4]. The epidemiological study on the virus brings in to notice the first case to be reported on December 2019 in China, which was then observed with the aggressive or violent form by January 2019 with increasing number of cases trans-

mitting in the other parts of the world [5,6]. By January 2019, approximately eighteen countries were reported to be infected with the virus emerged in China led to the declaration as “Public Health Emergency of International Concern” by World Health Organization (WHO) on Mar 11, 2020 [7]. As on Jul 9, 2021 there have been reported 185,291,530 confirmed cases with 4,010,834 fatal cases worldwide [8]. The entire world has to suffer from the huge numbers of challenges due to this global pandemic as all the vital sectors like health, education, economic, social, pharmaceutical, etc. have been widely affected. Unemployment, events cancellation, prohibited public places, declined foreign and domestic trades during the pandemic caused a huge fall in the global economy [9,10].

The novel SARS CoV-2 viral pathogens responsible for the global pandemic have been derived from the previously emerged strain reported in 2002–03 which are suspected to be transmitted into humans through several animal hosts such as bats, civets, pangolins and camels [11]. The clinical symptoms in the patients infected with coronaviruses may vary from moderate symptomatic to severe asymptomatic characteristics including headache, cough, cold, tiredness, aches, fever, loss of taste or smell, diarrhoea, discoloration of finger or toes, breathing difficulties to dysfunction of organs. The viruses such as SARS and MERS are transmitted into humans through the direct or indirect exposure of the respiratory secretions [12,13].

The large genome of the coronaviruses including 30 kb long nucleotide sequence has been comprised within the single stranded positive sense enveloped RNAs [14]. The crown like structural mor-

*Abbreviations:* ACE2, angiotensin converting enzyme 2; ADMET, absorption, distribution, metabolism, excretion and toxicity; BBB, blood-brain barrier; BOILED, brain or intestinal estimated permeation method; COVID-19, corona virus disease 2019; E, envelope protein; FDA, food and drugs administration; HBA, hydrogen bond acceptor; HBD, hydrogen bond donor; HERG, human ether-*a*-go-go-related gene; LOAEL, oral rat chronic toxicity; M, membrane protein; MD, molecular dynamics; N, nucleocapsid protein; NSPs, non-structural proteins; pp1a/b, polyproteins; RdRp, RNA dependent RNA polymerase; S, spike glycoprotein; SARS CoV-2, severe acute respiratory syndrome 2; ssRNA, single stranded ribonucleic acid; UTR, untranslated region; WHO, world health organization.

\* Corresponding author.

E-mail addresses: [tejas.dhameliya@lmcp.ac.in](mailto:tejas.dhameliya@lmcp.ac.in), [tmdhameliya@gmail.com](mailto:tmdhameliya@gmail.com) (T.M. Dhameliya).

<sup>1</sup> These authors contributed equally to this work.

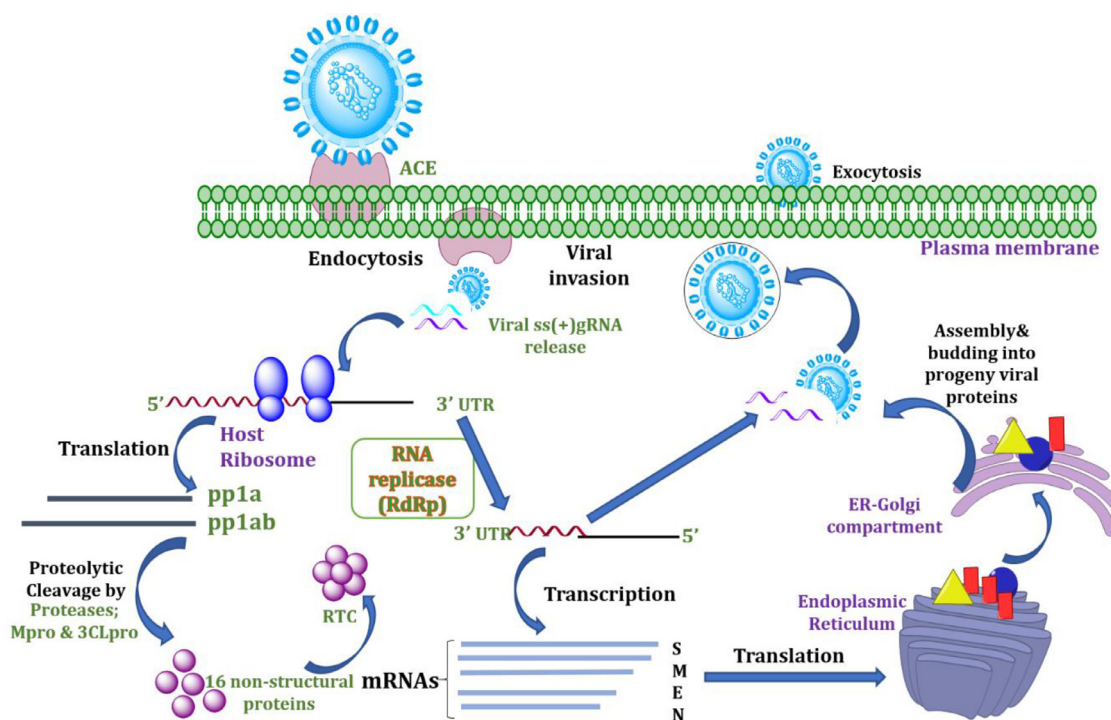


**Fig. 1.** Life cycle of corona virus inside the host cell. ACE2:Angiotensin Converting Enzyme 2; 3'UTR:Untranslated region; pp1a/pp1ab: polyproteins; S: spike glycoprotein; M: membrane protein; E: envelope protein; N: nucleocapsid protein.

phology of these viruses observed under electron microscope are due to the club-like glycoproteins [13]. The CoV belongs to the  $\beta$ -coronaviruses among the four major genres of the large family Nidovirales [15]. The critical insights into the viral pathogenesis and replication may shine a light towards the comprehensive understanding regarding the virus as presented in Fig. 1. The pathogenesis of corona virus begins with the fusion and attachment to the host receptor angiotensin converting enzyme-2 (ACE2) through its spike glycoprotein. Upon invasion and after releasing its genomic material inside the host cell, the genome gets translated into several polypeptides followed by the translation into sixteen non-structural polyproteins (NSPs). The 3' end of the sub-genomic RNA gets transcribed into several structural proteins which are assembled on the endoplasmic reticulum (ER) and golgi body to release the viral progenies outside the plasma membrane [16].

Despite of current antiviral strategies including the anti-viral agents and vaccines to combat the deadly coronavirus, these could not prove themselves effective against the virulent disease. In order to generate the scopes for effective inhibitors of SARS CoV-2, several drugs have been repurposed and implemented to combat this ailment, though they have not shown any reliable results necessitating the demand for some potential inhibitors [17,18]. In view of this fact, several vaccines containing live attenuated, RNA-DNA derived, viral vectored, protein contained and inactivated vaccines have been developed with positive results against the catastrophic virus, SARS CoV-2 [19]. In contrary, the vaccines under phase III trials have also been noted with several side effects after the vaccination such as headache, fatigue, chills, diarrhoea, arthralgia, myalgia, redness, itching, swelling, etc. [20] To exemplify, a nucleotide analog, remdesivir was declared under emergency use authorization by United States food and drug administration (USFDA) and was evaluated under *in vivo* and *in vitro* studies for the inhibition of viral replication inside the host body [21]. Despite of its efficacy, it has not been found effective solution to tackle the race for the inhibition of the deadly virus due to its impotency in patients

with immunodeficiency and heart failure, hypotension, respiratory dysfunction, as well as renal impairment [22].

The conventional approach to the drug design and development may take plenty of resources such as cost, time and manpower with no guarantee to afford the desired candidates with efficacy and potency. Therefore, the computer assisted drug design (CADD) have been preferred over several years above the traditional approaches reducing the cost-burden by benefiting the feasibility and improved results after removing the gap between chemical and biological science [23]. Among these CADD tools, the use of molecular modeling should not be undermined as they provide significant interactions of identified hits against their biological targets to understand their mode of action [24–28]. Recently, we have performed *in silico* screening of significant phytochemicals against RNA-dependent RNA Polymerase (RdRp) and main protease (Mpro) using molecular docking followed by their druggability using ADMET assay and stability of their complexes using molecular dynamics (MD) simulations in search of effective SARS CoV-2 inhibitors [29]. Motivated by the potential of computational chemistry and in search of potent inhibitors of SARS CoV-2, herein we have performed the virtual screening of total 267,324 ligands from 2020-01 Asinex EiteSynergy (91,473) and BioDesign (175,851) libraries using AutoDock Vina against RdRp using molecular docking followed by their further assessment using rules for druggability, ADMET assay and MD simulations.

## 2. Results and discussion

### 2.1. Analysis of protein structure

Xu et al. have reported the cryo-EM structure of the RdRp from SARS-CoV-2, co-crystallized with remdesivir having the resolution of 2.8 Å (PDB ID: 7BV2) [30,31]. In this complex, partial double-stranded RNA template was implanted into the central channel of the RdRp where remdesivir was covalently fused into the primer

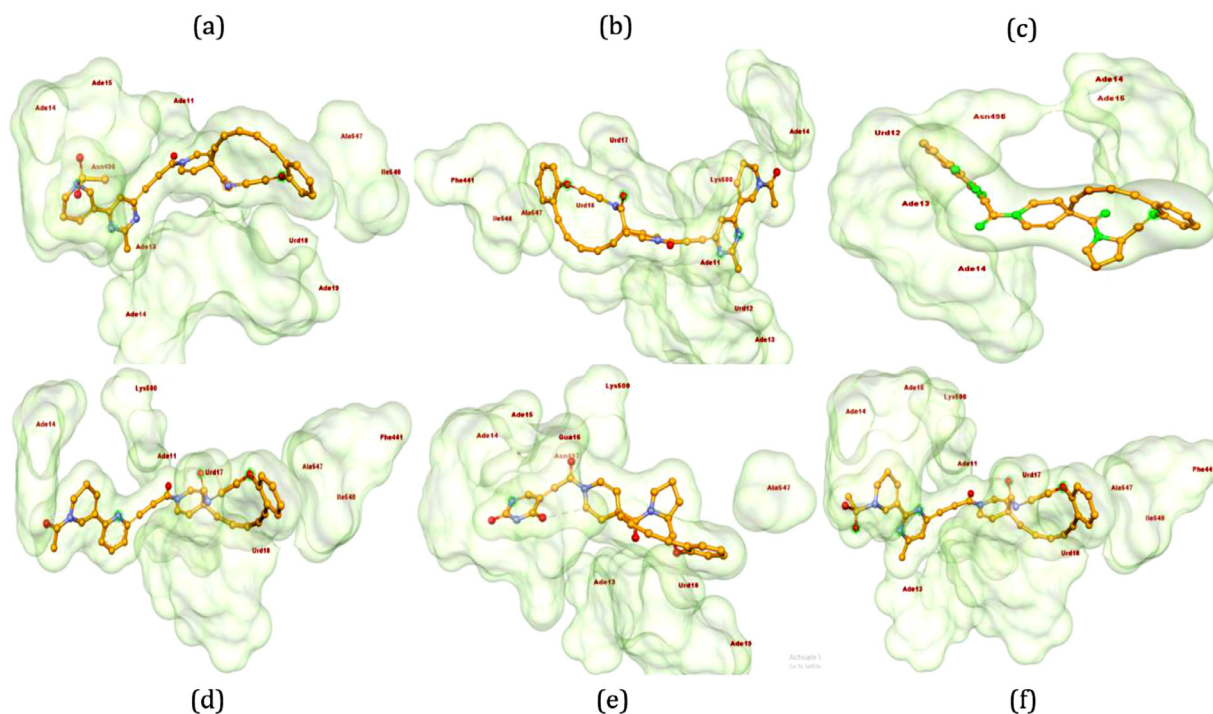


**Fig. 2.** The 3D-interactions of ligands **2** (a), **3** (b), **4** (c), **5** (d), **6** (e) and **7** (f) complexed with RdRp. Poses have been generated using Biovia Discovery Studio 2020 [38].

strand at the first replicated base pair and terminated the chain elongation. The core component of the viral replication complex is the non-structural proteins (nsp12) of the RdRp [32,33].

## 2.2. Molecular docking

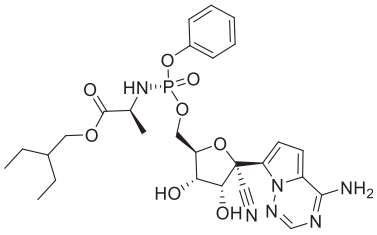
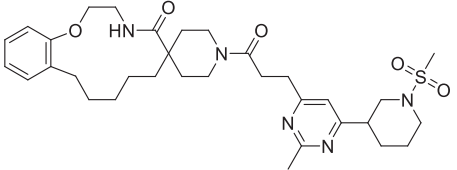
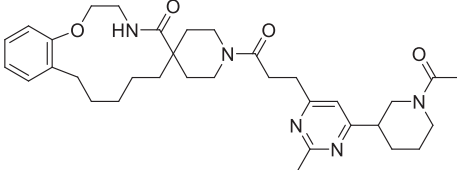
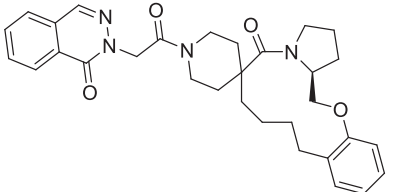
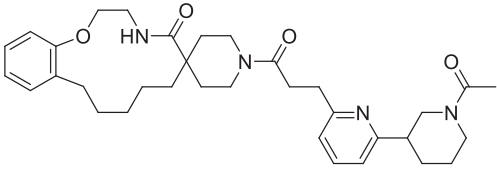
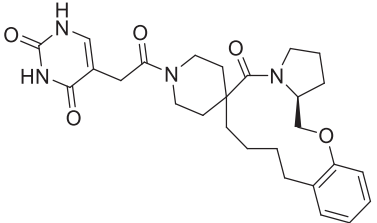
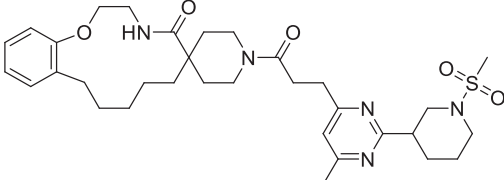
The molecular docking has been performed against the selected protein (PDB ID: 7BV2) [30] using AutoDock Vina [34] to evaluate the binding mode of ligand and interactions in the active site. The required 267,324 ligands have been obtained from 2020–01 Asinex EiteSynergy (91,473) and BioDesign (175,851) library from the Asinex online database, a part of PubChem database consists of small molecules, which can be easily synthesized in organic chemistry labs [35]. The preprocessed protein and ligands in PDBQT format have been used for the molecular docking process. The binding energy of the hit molecules (**2–22**) have been compared with the co-crystallized ligand remdesivir (**1**, Table 1, Entry 1). Further, these hits (**2–22**) have been found with better binding energy as compared to other promising RdRp inhibitors such as ribavirin (**23**), penciclovir (**24**), favipravir (**25**), [36] molnupiravir (**26**) and sofosbuvir (**27**) [37]. Total twenty-one identified macrocyclic hits have been found to possess binding energy lesser than  $-12.5$  Kcal/mol and presented in Table 1 and their 2D-possess with the formed interactions have been presented in Figs. S1–S4 (see supporting information).

The 3D-poses of identified ligands **2–7** bound at the active site of RdRp have been generated using Biovia Discovery Studio 2020 [38] and presented in Fig. 2a–f. Compound **2** formed conventional hydrogen bonds (HB) with the amino acid Asn496 from chain A and nucleotides Ade11 and Ade13 of chain P, Ade14, Ade15 and Ade19 of chain T. Further, it formed van der Waals interactions with Ile548 and Ade14 of chain P,  $\pi$ -anion interaction with Urd18 (chain P),  $\pi$ -alkyl interaction with Ala547, Ade13 and Ade14 (chain T, Fig. 2a). Additionally, the presence of sulfonyl group in the structure of **2** could lead the formation of  $\pi$ -sulfur interaction with Ade15 of chain P. Pyrimidine derivative **3** made conventional HB with Ade14 of chain P and Ade11 of chain T, C-H

bond with Lys500 and Urd12 of chain T,  $\pi$ - $\pi$  bond with Phe441,  $\pi$ -alkyl bond with Ala547 and Ile548 along with  $\pi$ -anion bond with Urd17 of chain P (Fig. 2b). Compound **4** formed conventional HB with the amino acid, Asn496 and nucleotides, Ade13 and Ade14 of chain P and Ade14 and 15 of chain T. Additionally, it formed  $\pi$ - $\pi$  bond with Urd12 of chain T (Fig. 2c). By the replacement of 2-methylpyrimidine ring of compound **3** with pyridine ring in compound **5** retained almost similar interactions including van der Waals bond (Lys500),  $\pi$ - $\pi$  bond (Phe441,  $\pi$ -alkyl bond with Ala547 and Ile548),  $\pi$ -anion bond (Urd17 and Urd18 of chain P, Fig. 2d). Compound **6** found to form conventional HB with Ade14, Gua16 and Ade19 of chain P, Ade13 of chain T, Lys500 and Asn497. It also formed C-H bond with Asn497,  $\pi$ -anion bond with Ade19 of chain P and  $\pi$ -alkyl bond with Ala547 and Urd18 of chain P (Fig. 2e). *N*-Methylsulfonyl piperidine substituted compound **7** interacted at the active site of RdRp by forming  $\pi$ -alkyl bond (Ala547, Ile548 and Ade13 of chain T),  $\pi$ -sulfur bond (Ade14 of chain P),  $\pi$ -anion bond (Urd17 and Urd18 of chain P), C-H bond (Lys500) and conventional HB (Ade11 of chain T and Ade14 and 15 of chain P, Fig. 2f). In general, these interactions with the ligands have supported our hypothesis on the tight binding of identified ligands into the active site of protein.

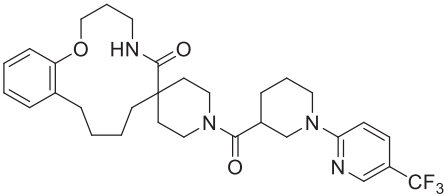
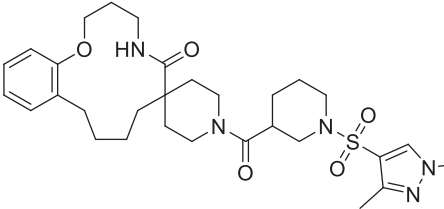
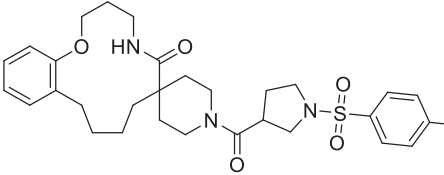
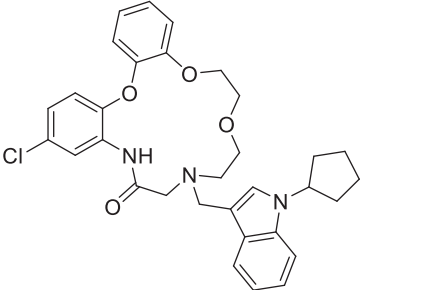
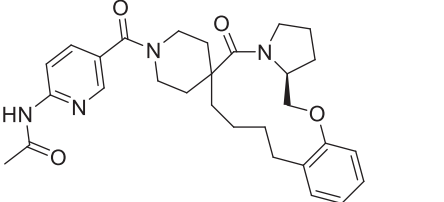
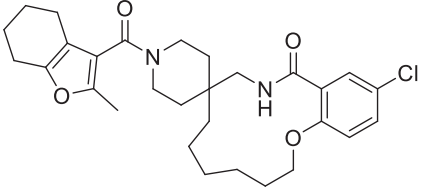
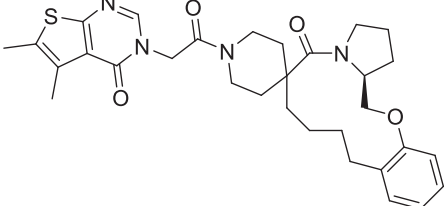
2,4-Disubstituted pyridine derivative **8** has been found with binding energy of  $-12.8$  Kcal/mol (Table 1) due to interaction with RdRp including  $\pi$ -alkyl bond with Ade19 of chain P and conventional HB with Ade11 of chain T, Ade14 and Ade19 of chain P (Fig. 3a). 1,3-Dimethyl-1*H*-pyrazol-4-yl sulfonyl derivative compound **9** (Fig. 3b) found to bind tightly through the formation of  $\pi$ -anion bond with Urd13 of chain P, non-polar C-H bond with Urd18 of chain P,  $\pi$ -sulfur bond with Ade19 of chain P and HB with Ade11 (chain T) Ade14 and Ade19 (chain P). Interactions including C-H bond (Lys500),  $\pi$ -alkyl bond (Ala547),  $\pi$ -sulfur bond (Ade14 of chain T),  $\pi$ -anion bonds (Asp845 and Urd18 of chain P) and conventional HB (Ade13, Ade14 of chain T and Gua16, Ade15 of chain P) have been found with the docked complex of 1-sulfonyl pyrrolidine-3-carboxamide **10** against RdRp (Fig. 3c) with similar

**Table 1**  
The identified hits (2–22) having more binding energy than clinically used remdesivir (1) and other RdRp inhibitors (23–27).

Compound No.	Dataset ID	2D-Structure	Binding energy (Kcal/mol)
1	Remdesivir		-9.2
2	LAS 51620435		-13.1
3	LAS 51620429		-13
4	LAS 51609341		-13
5	LAS 51620411		-12.9
6	LAS 51609377		-12.8
7	LAS 51620382		-12.8

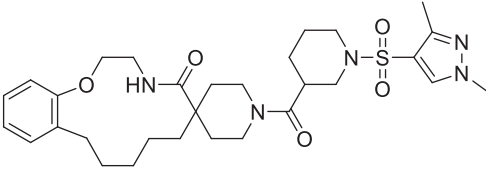
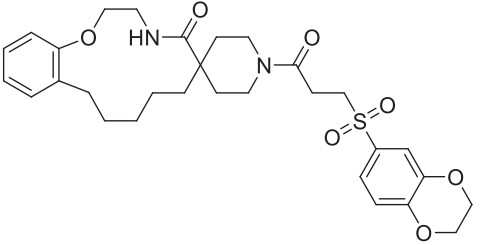
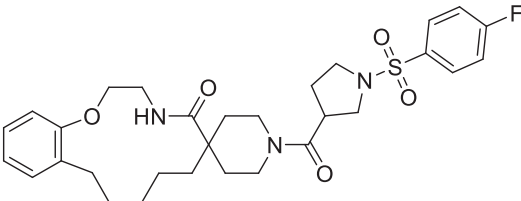
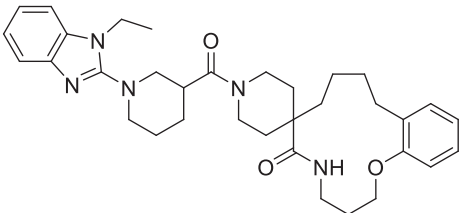
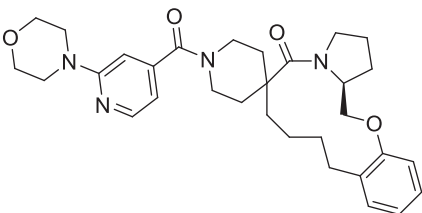
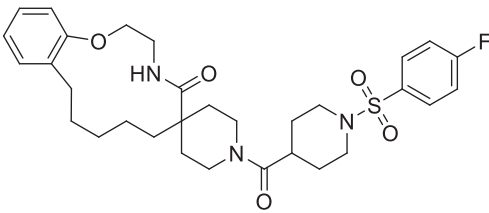
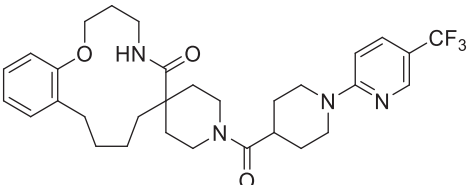
(continued on next page)

**Table 1** (continued)

Compound No.	Dataset ID	2D-Structure	Binding energy (Kcal/mol)
8	LAS 51624260		-12.8
9	LAS 51624264		-12.8
10	LAS 51624295		-12.8
11	LAS 52131039		-12.8
12	LAS 51609335		-12.7
13	LAS 51614073		-12.7
14	LAS 51609336		-12.6

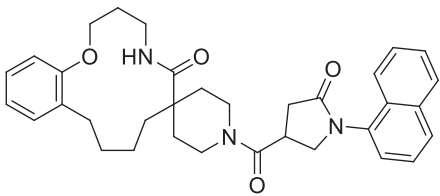
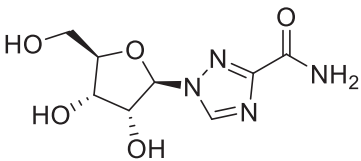
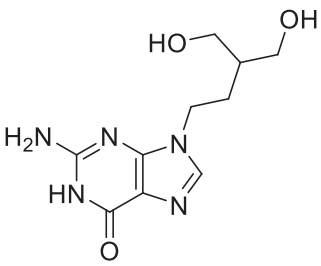
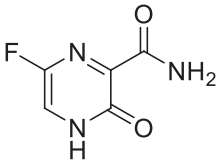
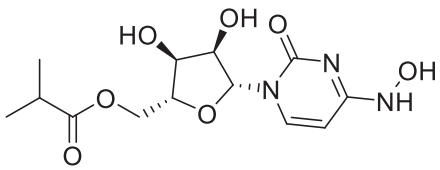
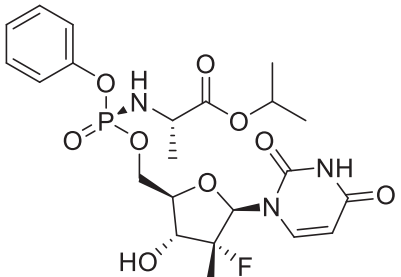
(continued on next page)

**Table 1** (continued)

Compound No.	Dataset ID	2D-Structure	Binding energy (Kcal/mol)
15	LAS 51620402		-12.6
16	LAS 51620430		-12.6
17	LAS 51620433		-12.6
18	LAS 51624245		-12.6
19	LAS 51609330		-12.5
20	LAS 51620424		-12.5
21	LAS 51624284		-12.5

(continued on next page)

Table 1 (continued)

Compound No.	Dataset ID	2D-Structure	Binding energy (Kcal/mol)
22	LAS 51624301		-12.5
23	Ribavirin		-7.4
24	Penciclovir		-7.2
25	Favipiravir		-6.7
26	Molnupiravir		-10
27	Sofosbuvir		-8.7

binding energy. Apart from the interactions including conventional HB (Ade14 of *P* chain, Ade13 and Ade14 of *T* chain), two  $\pi$ - $\pi$  bonds (Urd12) and  $\pi$ -alkyl bond (Urd10 from chain *T*), *N*-cyclophenyl indole derivative **11** formed halogen interactions between chlorine atom present in it with Cyt15 and Ade14 of chain *T* (Fig. 3d). The replacement of pyrimidine-2,4(1*H*,3*H*)-dione-6-methyl in ligand **6** with pyridin-2-yl-acetamide in **12** has been resulted in almost similar binding energy (-12.8 and -12.7 kcal/mol, respectively) along the with formation of  $\pi$ -anion bond with Ade19 of chain *P*,  $\pi$ -alkyl bond with Ala547 and Urd18 of chain *P*, conventional HB with Ade14, Ade15 and Ade19 belonging to chain *P* (Fig. 3e). Several  $\pi$ -

alkyl interactions are found in docked complex of compound **13** with amino acids Phe441, Ile548, Lys500, nucleotides Urd17, Gua16 (chain *P*) and Ade11, Urd12 (chain *T*). Further, ligand **13** formed conventional HB with Lys545, Arg836 and Ade14 of chain *T* and  $\pi$ -anion bond with Urd18 of *T* chain and  $\pi$ - $\sigma$  bond with Ala547 (Fig. 3f).

Compound **14**, with binding energy of -12.6 kcal/mol, formed conventional HB with Ade19 of chain *P* and Ade11, Ade14 and Cyt15 of chain *T*,  $\pi$ -anion bond with Urd13 of chain *P*. Additionally, nucleotide Urd18 has found with  $\pi$ - $\pi$  bond,  $\pi$ -sulfur bond and  $\pi$ -alkyl bond with the ligand **14** (Fig. 4a). Compound **15**, a



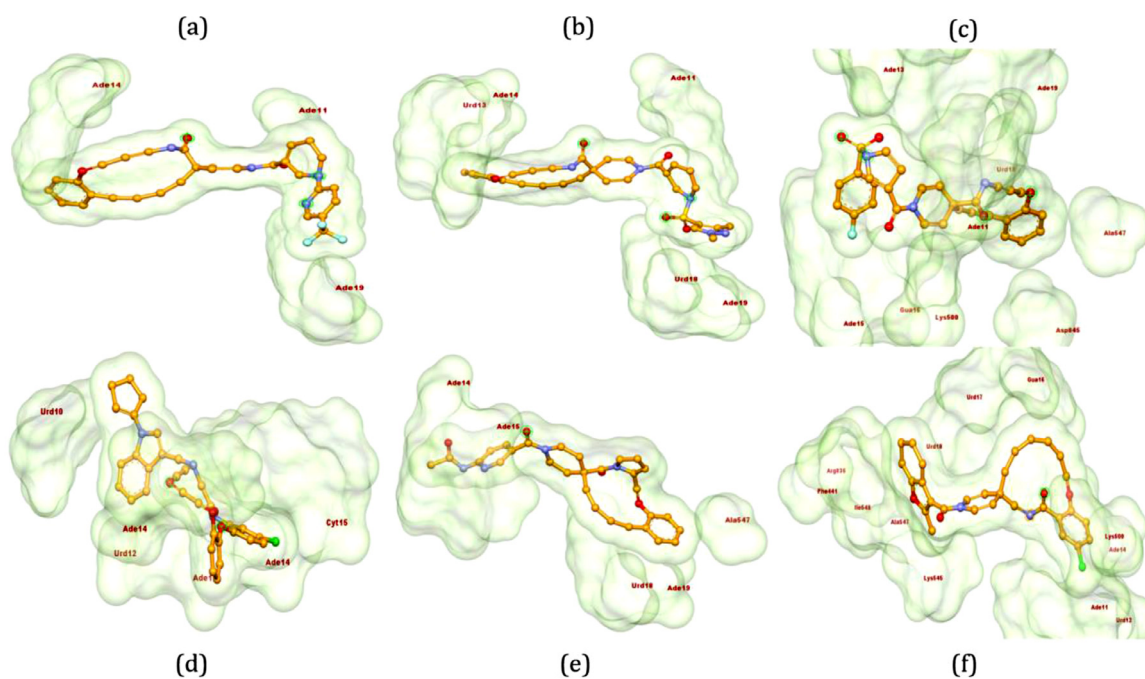


**Fig. 3.** 3-D interactions of ligands **8** (a), **9** (b), **10** (c), **11** (d), **12** (e) and **13** (f) with RdRp (PDB ID: 7BV2). Interactive poses of hits have been generated using Biovia Discovery Studio 2020 [38].

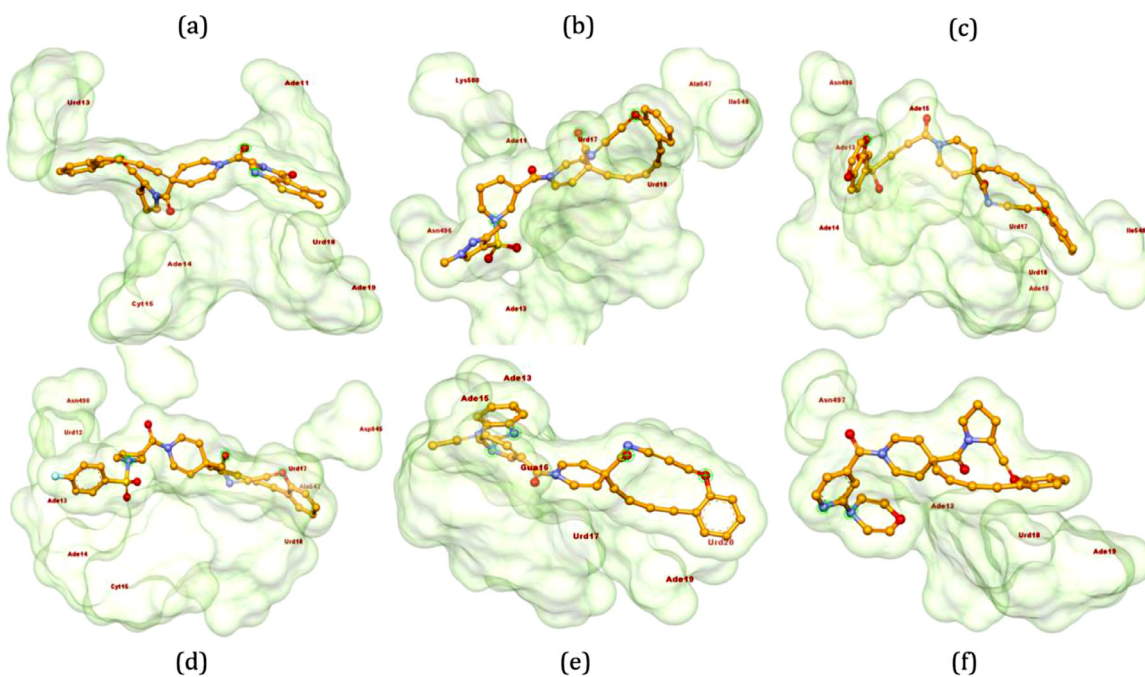


**Fig. 4.** 3D interactions of ligands compound **14** (a), compound **15** (b), compound **16** (c), compound **17** (d), compound **18** (e) and compound **19** (f) with 7BV2. Poses have been generated using Biovia Discovery Studio 2020 [38].

metamer of compound **9**, formed completely dissimilar interactions in comparison with **9** such as C-H bond with Lys500,  $\pi$ -sulfur bond with Ade13 of *T* chain,  $\pi$ -alkyl bonds with Ala547 and Ile548,  $\pi$ -anion bonds with Urd17 and Urd18 from chain *P* and conventional HB with Asn496, Ade11 and Ade13 of chain *T* (Fig. 4b). Next, 2,3-dihydrobenzo[*b*][1,4]dioxin-6-sulfonyl derivative **16** found to form  $\pi$ -sulfur bond with Ade14 of chain *T*,  $\pi$ -alkyl bond with Ile548,  $\pi$ -anion bond with Urd17 and Urd18 of chain *P* and HBs with the amino acid Asn496 and nucleotides Ade15

and Ade19 from *P* chain and Ade13 and 14 from *T* chain (Fig. 4c). Compound **17** being *N*-(4-fluorophenylsulfonyl)pyrrolidine derivative formed two  $\pi$ -alkyl bonds (Ala547),  $\pi$ -sulfur bond (Ade17 of chain *T*), C-H bonds (Lys500 and Urd12 of chain *T*),  $\pi$ -anion bonds (Asp845, Urd17 and 18 from *P* chain), conventional HB (Ade13, Ade14 and Cyt15 of chain *T*). Further, 4-fluoro on phenyl ring interacted with Asn496 through halogen interactions (Fig. 4d). *N*-Ethyl 2-substituted benzo[*d*]imidazole derivative **18** interacted with the protein through C-H bonds with Gua16 and Urd17 of chain *P*



**Table 2**  
Physicochemical properties of the macrocyclic hits (2–22) and marketed drug, remdesivir (1).<sup>a</sup>

Comp No.	MW <sup>b</sup>	HBD <sup>c</sup>	HBA <sup>d</sup>	RB <sup>e</sup>	Log P <sup>f</sup>	No. of violations <sup>g</sup>
1	602.58	4	12	14	2.31	2
2	625.82	1	8	6	3.78	1
3	589.77	1	6	6	4.36	1
4	528.64	0	5	3	3.80	1
5	574.75	1	5	6	4.66	1
6	494.58	2	5	3	2.01	0
7	625.82	1	8	6	3.78	1
8	572.66	1	7	4	5.24	2
9	585.76	1	7	4	3.05	1
10	571.70	1	7	4	3.76	1
11	560.08	1	5	3	7.05	2
12	504.62	1	5	4	4.06	1
13	513.07	1	4	2	6.12	2
14	562.72	0	5	3	4.48	1
15	585.76	1	7	4	3.05	1
16	570.70	1	7	5	3.54	1
17	571.70	1	7	4	3.76	1
18	571.75	1	4	4	5.19	2
19	532.67	0	5	3	3.94	1
20	585.73	1	7	4	4.15	1
21	572.66	1	7	4	5.24	2
22	553.69	1	4	3	5.11	2

<sup>a</sup> Parameters calculated using pkCSM [40,41],

<sup>b</sup> Molecular weight ( $\leq 500$  Da),

<sup>c</sup> Number of hydrogen bond donors ( $\leq 5$ ),

<sup>d</sup> Number of hydrogen bond acceptors ( $\leq 10$ ),

<sup>e</sup> Number of rotational bonds ( $\leq 10$ ),

<sup>f</sup> Partition coefficient in oil to water ( $\leq 5$ ).

130) and atoms (20–70) to be the good drug candidate [46] and all the hits meet the suggested properties. However, as compared to Remdesivir, the identified hits may have potential to act as a good

drug candidate in the future as they obey the rules for druggability and drug-likeness.

Next, we have studied the various ADMET (absorption, distribution, metabolism, excretion and toxicity) parameters like water solubility (Ali log  $S$ ), molar refractivity (MR), topological polar surface area (tPSA), CaCO<sub>2</sub> cell permeability, intestinal absorption, volume of distribution ( $V_d$ ), unbound fraction of drug and ability to inhibit the P-glycoprotein substrate for the identified hits. All the molecules have satisfied the criteria for the Ali log  $S$ , tPSA and CaCO<sub>2</sub> cell permeability. Most of the hits with sufficient human intestinal absorption indicated their better oral bioavailability. All the hits also qualified the criteria for  $V_d$  along with the inhibition of the P-glycoprotein substrates. Further, we analyzed the additional parameters to predict the metabolism, excretion and toxicity profile of remdesivir and these hits (Table 4). Most of the molecules inhibited CYP2D6 but not CYP3A4 along with medium renal clearance except compound 16 and 22 (with low clearance). All the hits except hits 4, 5, 18 were found as the substrates for renal uptake transporter in proximal convoluted tubule (OCT2). All the hits were found non-cytotoxic (hERG cell line), non-mutagenic (AMES toxicity), non-toxic to dermis (skin sensitization) and found safe through prediction of oral rat acute and (LD<sub>50</sub>) chronic toxicity (LOAEL). Thus, these macrocyclic hits (2–22) might be good and successful drug candidates in the future.

The Brain Or Intestinal EstimatedD permeation method (BOILED-Egg) provide the *in silico* estimation of accessibility of molecules to gastrointestinal (GI) tract and blood-brain barrier [47]. Hence, we also become interested to predict the permeability of the identified macrocyclic hits using SwissADME [39]. The boiled egg model revealed all the hit molecules possessed satisfactory GI absorption along with inhibition of the P-glycoprotein, a protein responsible for efflux of drugs from cells (Fig. 7). All the compounds (except 19) were found with probability of permeation to BBB and hence-

**Table 3**  
Predicted absorption and distribution properties of the hits (2–22) and remdesivir (1).<sup>a</sup>

Comp No.	Ali log $S^b$	MR <sup>c</sup>	tPSA ( $\text{\AA}^2$ ) <sup>d</sup>	CaCO <sub>2</sub> permeability <sup>e</sup>	Human intestinal absorption (% absorbed) <sup>f</sup>	VD <sub>ss</sub> (Human) <sup>g</sup>	Fraction unbound (Human) <sup>h</sup>	P-gp inhibition (yes/no) <sup>i</sup>
1	-6.01	150.43	213.36	0.51	69.44	-0.38	0.03	Yes
2	-5.89	182.34	130.18	0.99	98.37	-0.40	0.00	Yes
3	-5.57	178.39	104.73	1.00	97.33	-0.09	0.02	Yes
4	-5.37	157.77	84.74	1.49	94.72	0.28	0.00	Yes
5	-5.56	175.62	91.84	0.98	89.36	0.04	0.01	Yes
6	-3.95	143.15	115.57	1.04	78.89	-0.13	0.21	Yes
7	-5.89	182.34	130.18	0.90	92.22	-0.47	0.00	Yes
8	-6.56	161.6	74.77	0.79	90.74	-0.02	0.00	Yes
9	-5.05	168.38	122.22	0.95	86.35	-0.45	0.00	Yes
10	-5.75	161.52	104.4	0.95	95.03	-0.31	0.00	Yes
11	-6.79	165.08	64.96	1.03	91.72	0.55	0.13	Yes
12	-4.89	149.43	91.84	0.88	95.13	0.06	0.06	Yes
13	-7.47	149.63	71.78	0.65	89.23	0.46	0.00	Yes
14	-6.77	165.58	112.98	0.92	93.39	0.14	0.02	Yes
15	-5.24	168.38	122.22	1.02	86.64	-0.51	0.00	Yes
16	-5.78	158.12	119.62	1.13	87.27	-0.31	0.00	Yes
17	-5.94	161.52	104.4	1.02	95.32	-0.39	0.00	Yes
18	-6.66	178.16	79.7	0.74	90.82	0.61	0.02	Yes
19	-5.15	160.85	75.21	1.45	96.05	0.02	0.00	Yes
20	-6.31	166.33	104.4	1.00	100	-0.39	0.00	Yes
21	-6.56	161.6	74.77	0.77	90.62	-0.19	0.00	Yes
22	-6.19	171.7	78.95	0.76	93.19	0.48	0.00	Yes

<sup>a</sup> Parameters calculated using pkCSM [40].

<sup>b</sup> Aqueous solubility descriptor ( $\leq 0$ ),

<sup>c</sup> molar refractivity ( $\leq 155$ ),

<sup>d</sup> topological polar surface area ( $\leq 150 \text{\AA}^2$ ),

<sup>e</sup> Caco-2 cell permeability ( $\log P_{app}$  in  $10^{-6}$  cm/s  $> 0.09$ ),

<sup>f</sup> absorption (human, %  $> 30$ ),

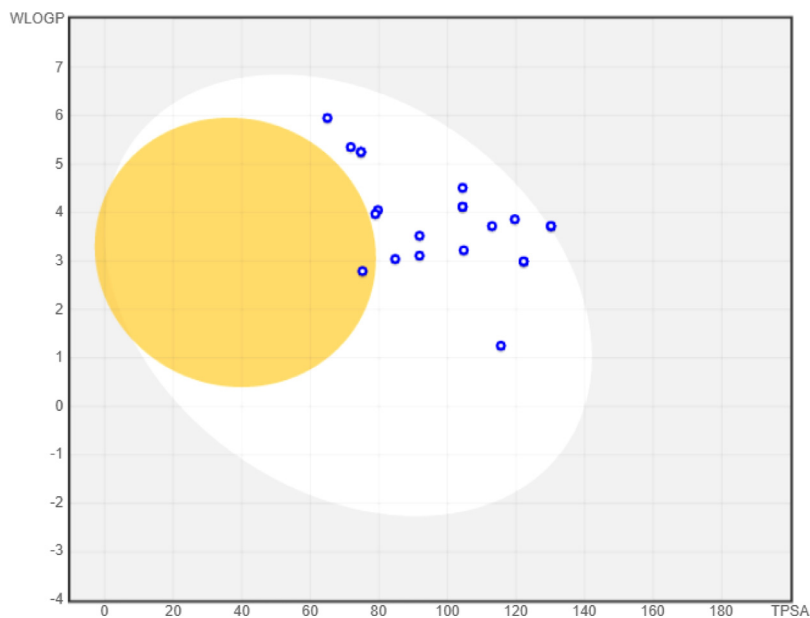
<sup>g</sup> volume of distribution (human, log L/kg) (low if  $< -0.15$  and high if  $> 0.45$ ),

<sup>h</sup> fraction unbound, and

<sup>i</sup> ability to inhibit the P-glycoprotein.

**Table 4**  
Metabolism, excretion and safety parameters of remdesivir (1) and identified hits (2–22).<sup>a</sup>

Comp No.	CYP2D6 inhibitor <sup>b</sup>	CYP3A4 inhibitor <sup>c</sup>	CL <sub>r</sub> <sup>d</sup>	Renal OCT2 substrate <sup>e</sup>	AMES toxicity <sup>f</sup>	hERG I toxicity <sup>g</sup>	LD <sub>50</sub> <sup>h</sup>	LOAEL <sup>i</sup>	Skin sensitization <sup>j</sup>
1	No	No	0.16	No	No	No	2.25	2.27	No
2	No	Yes	0.56	No	No	No	3.09	1.54	No
3	No	Yes	0.50	No	No	No	3.20	1.33	No
4	No	Yes	0.27	Yes	No	No	2.88	-0.08	No
5	No	Yes	0.49	Yes	No	No	3.34	-0.45	No
6	No	Yes	0.42	No	No	No	2.40	0.92	No
7	No	Yes	0.54	No	No	No	2.95	1.51	No
8	No	Yes	0.11	No	No	No	2.70	0.80	No
9	No	Yes	0.36	No	No	No	2.97	1.78	No
10	No	Yes	0.37	No	No	No	2.80	1.44	No
11	No	Yes	0.55	No	No	No	3.24	-0.19	No
12	No	Yes	0.37	No	No	No	2.65	1.60	No
13	No	Yes	-0.09	No	No	No	2.49	0.71	No
14	No	Yes	0.05	No	No	No	2.92	-0.42	No
15	No	Yes	0.40	No	No	No	3.11	1.63	No
16	No	Yes	0.43	No	No	No	3.05	1.69	No
17	No	Yes	0.40	No	No	No	2.98	0.94	No
18	No	Yes	0.44	Yes	Yes	No	2.37	1.47	No
19	No	Yes	0.40	No	No	No	3.18	-0.12	No
20	No	Yes	0.41	No	No	No	3.03	0.97	No
21	No	Yes	0.17	No	Yes	No	3.00	-0.08	No
22	No	Yes	-0.03	No	No	No	2.46	1.79	No

<sup>a</sup> Parameters calculated using pkCSM [40].<sup>b</sup> ability to inhibit CYP2D6 enzyme,<sup>c</sup> ability to inhibit CYP3A4 enzyme,<sup>d</sup> total renal clearance; high (> 1 mL/min/kg), medium (> 0.1 to < 1 mL/min/kg) or low (≤ 0.1 mL/min/kg),<sup>e</sup> ability to inhibit renal OCT2 substrate;<sup>f</sup> AMES toxicity;<sup>g</sup> hERG I toxicity;<sup>h</sup> oral rat acute toxicity (LD<sub>50</sub>);<sup>i</sup> oral rat chronic toxicity (LOAEL);<sup>j</sup> skin sensitisation.**Fig. 7.** BOILED egg model of hit molecules (2–22) generated with the help of SwissADME. The yellow and colorless regions indicate BBB and GI permeability, respectively. The blue circles indicate inhibition of P-glycoprotein.

forth, the least chances of neurotoxicity of CNS with the proposed compounds 2–18 and 20–22 may be approximated.

#### 2.4. MD simulation

To study the stability of ligand into the binding site of protein, molecular dynamics (MD) simulations provide the better understanding of ligand through several statistical parameters [48,49]. Several scientific literatures support the reliability and satisfactory

stability for the MD run (≤ 10 ns) through *in silico* endeavor [50–55]. In a similar line of approach, the hit complexes obtained from the evaluation of ADMET and drug-likeness properties, were subjected for MD simulations using GROMACS 2020.1 to assess the stability of the ligands (2 and 3) in the active site of docked complex at various time points up to 10 ns [56,57].

Next, we subjected the complex of compound 2 to MD simulation studies and the graphical representation of plots of statistical parameters has been presented in Fig. 8. The ligand-receptor com-

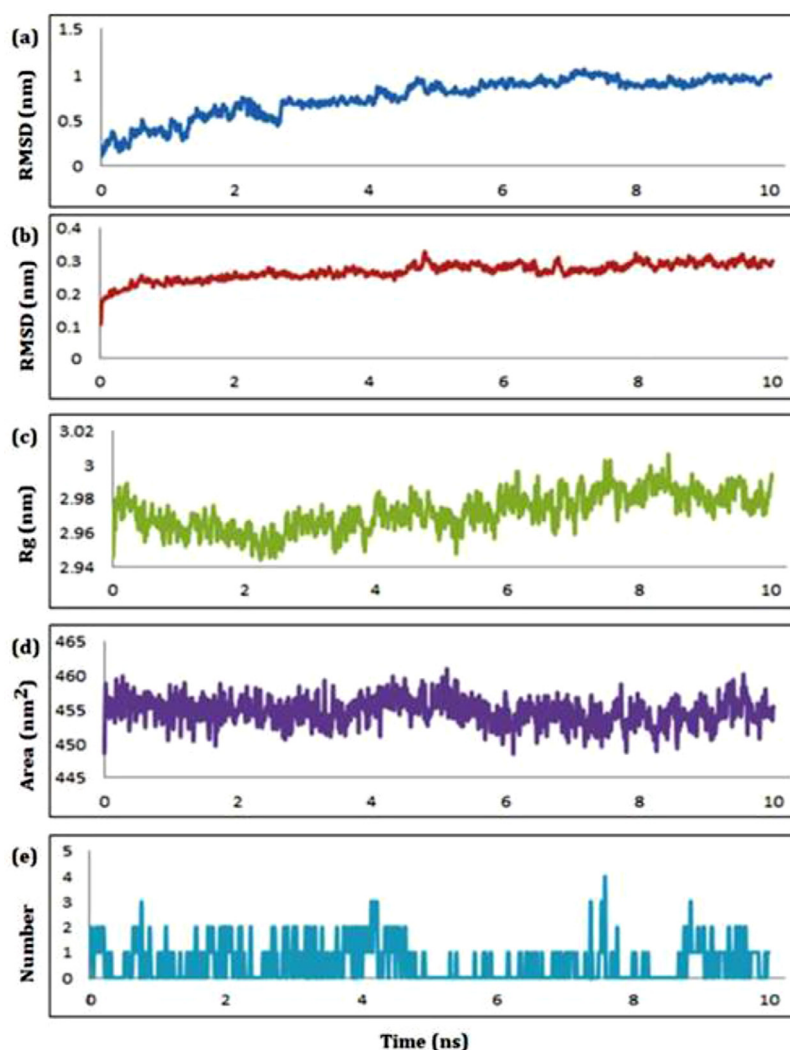


Fig. 8. The schematic plots of RMSD-L (a), RMSD-P (b), RoG (c), SASA (d) and HB (e) for the complex of compound 2 with RdRp.

Table 5

The electrostatic steric interactions (KJ/mol) for the complex of respective compounds (2 and 3) with RdRp protein.

Compd. No.	Energy (KJ/mol)	
	Electrostatic interaction (Coul-SR)	van der Waals/Hydrophobic interactions (LJ-SR)
2	-48.7869 ± 4.6	-115.263 ± 9.1
3	-32.4944 ± 8.6	-108.078 ± 8.1

plex of **2** with RdRp was found with root mean square deviation (RMSD) value with an average of 0.757 nm (Fig. 8a) for the ligand and 0.267 nm (Fig. 8b) for the protein which indicate the stability of the ligand with least deviation in the active site of remdesivir. The radius of gyration (RoG) for the same complex ranging from 2.94 to 3.01 nm with an average of 2.972 nm (Fig. 8c) indicated the compactness of the complex. The plots of solvent assessable surface area (SASA) and hydrogen bonds has been presented in Fig. 8d and Fig. 8e, respectively. The surface area accessed by the solvent molecules was found within the satisfactory range from 447–461 nm<sup>2</sup> with an average of 454.72 nm<sup>2</sup> (Fig. 8d). From the plot of number of HB vs simulation time, maximum four HB were found between the ligand and receptor within the time period of 10 ns (Fig. 8e).

The satisfactory stability of the ligand with least deviation in the active site of complex has been evident from RMSD value

with an average of 0.942 nm (ligand, Fig. 9a) and 0.270 nm (protein, Fig. 9b) for the ligand-receptor complex of compound **3** with RdRp. The RoG for the same complex was found in the range of 2.94–3.00 nm with an average of 2.966 nm (Fig. 9c) indicating their compactness. The surface area accessed by the solvent/water molecules was found within the range from 446–460 nm<sup>2</sup> with an average of 454.215 nm<sup>2</sup> (Fig. 9d). From the plot of number of HB vs time, maximum two HBs were found between the ligand and receptor within the time period of 10 ns (Fig. 9e). The electrostatic (coulombic short-range, Coul-SR) and van der Waals/hydrophobic (LJ-SR) energies have been represented in Table 5 for the complexes of identified hits **2** and **3** with RdRp. These complexes have been observed to be stabilized by the van der Waals or hydrophobic interactions significantly over the electrostatic or coulombic contributions.

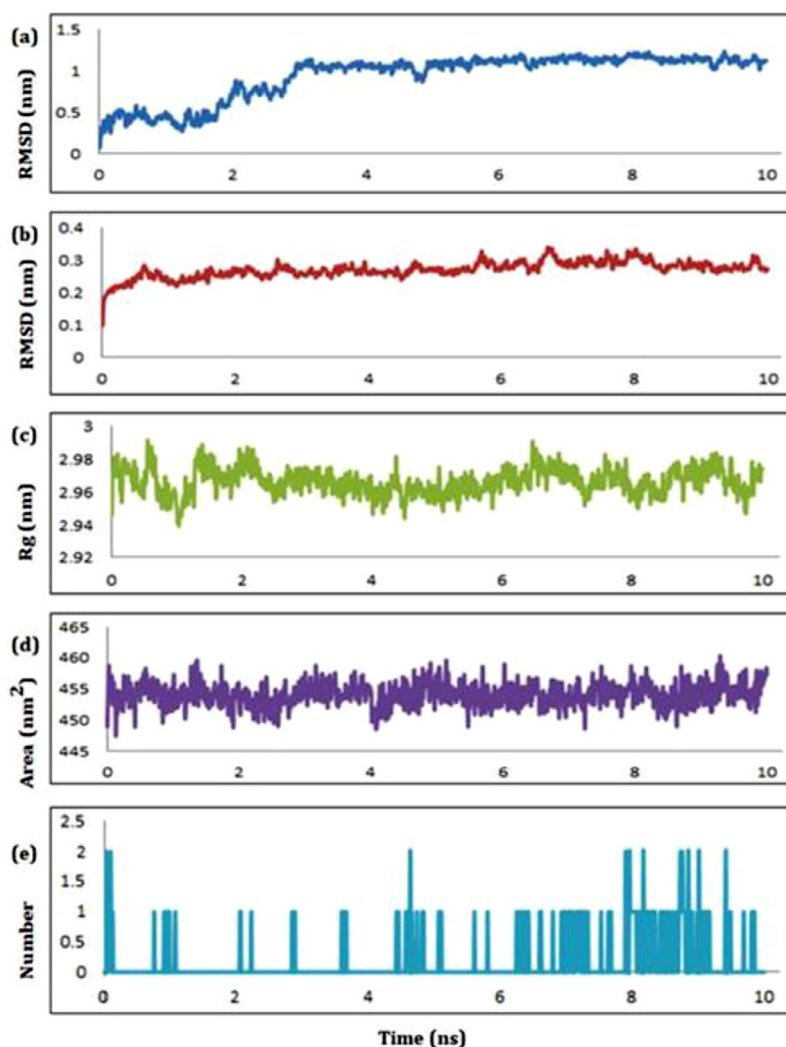


Fig. 9. The schematic plots of RMSD-L (a), RMSD-P (b), RoG (c), SASA (d) and HB (e) for the complex of compound **3** with RdRp.

### 3. Conclusion

In conclusion, the *in silico* based virtual screening of total 267,324 ligands from 2020-01 Asinex EliteSynergy (91,473) and BioDesign (175,851) libraries against RdRp using AutoDock Vina lead to discovery of twenty-one macrocyclic hits (**2–22**) with better binding energy than remdesivir (**1**), clinically used SARS CoV-2 inhibitor. The several interactions between ligand and protein helped to understand their binding mode into the active site of protein. The drug-likeness and druggability studied using several rules for druggability and analysis of ADMET profiles of these hits (**2–22**) revealed the better bioavailability and safety profile than **1**. MD simulation studies up to 10 ns using GROMACS 2020.1 of the top two hits (**2** and **3**) indicated their stability into the active site of complex. Further, the structural modifications of these molecules may have the scope with significant inhibition of SARS CoV-2 in future.

### Experimental section

#### Collection and preparation of data

The 3-dimensional structure of the SARS-CoV-2 RdRp evaluated through cryo electron microscopy (resolution: 2.8 Å) having antiviral remdesivir as a co-crystallised inhibitor (PDB ID: 7BV2) was obtained from RCSB protein data bank [30]. The protein was

prepared for further molecular modelling using AutoDock Vina [58]. All the water molecules were deleted along with addition of polar hydrogen atoms and Kollman charges to complete the protein in terms of polarity and charges, respectively. The generation of the receptor grid box around the macromolecule of co-crystallised ligand remdesivir was achieved with the size of  $90.768 \times 99.896 \times 99.788$  Å (x, y and z) and the co-ordinates of centers  $70 \times 70 \times 70$  Å (x, y, and z). The prepared protein has been kept in PDBQT format which has been further used for the molecular docking. The present docking protocol has been validated by docking of remdesivir using the same and observed with RMSD of less than 1.

The Asinex BioDesign library 2020.1 having 175,851 molecules and Asinex EliteSynergy having 91,473 molecules was downloaded from Asinex database [35]. All the ligand molecules have been optimized and converted into PDBQT format using OpenBabel and further used for molecular docking process [59].

#### Molecular docking

The multi-ligand molecular docking was performed using the prepared protein using AutoDock Vina to reveal the binding affinity and interactions of the ligands with RdRp protein (PDB ID: 7BV2) [30]. All the ligands (267,324) were docked on the site using the optimized grid box and ten poses per ligand were generated. The

docked pose of remdesivir was compared with the co-crystallized inhibitor remdesivir to validate the present docking protocol. The docking interactions of hits were visualized and analyzed using Biovia Discovery studio 2020 [38]. The 2D interactions of docked compounds (**2–22**) with RdRp have been presented in supporting information (Figs S1–S4).

#### Analysis of physicochemical properties, drug-likeness and ADMET parameters

Various physicochemical properties like molecular weight, number of hydrogen bond donors, number of hydrogen bond acceptors, oil to water partition co-efficient and number of rotational bonds of the selected hits (**2–22**) and remdesivir (**1**) were studied using Swiss ADME [39] and pkCSM [40,41]. Several rules such as Lipinski's rule of 5, Ghose rule, Veber's rule, Egan's rule and Muegge's rule were applied to the selected hits using the SwissADME to ensure their druggability and to identify numbers of violated parameters. The ADMET properties like water solubility, molar refractivity, topological polar surface area, CaCO<sub>2</sub> cell permeability, intestinal absorption, volume of distribution, fraction unbound, total renal clearance, hepatotoxicity and ability to inhibit the P-glycoprotein were also studied using pkCSM.

#### Molecular dynamics (MD) simulation

Two molecules (**2** and **3**), obtained from the manual analysis of the hits found from the results of molecular docking and ADMET analysis, were selected for MD simulation using GROningen Machine for Chemical Simulations (GROMACS) 2020.1 [56,57] software. CHARMM36 (Chemistry at Harvard Macromolecular Mechanics) as an all atom force field [60] and CHARMM General Force Field (CGenFF) server to retrieve the topology of (**2** and **3**) were used [61,62]. After solvation (TIP3P water model), neutralization (Na<sup>+</sup> and Cl<sup>-</sup> ions), equilibration [canonical (NVT) and isobaric-isothermic (NPT) ensemble for 100 ps], the complexes were subjected to molecular dynamics run for 10 ns. By analyzing the plots of temperature, pressure and energy equilibria of the trajectories (Figs S5 and S6, see supporting information), we found the system satisfactorily equilibrated.

#### Declaration of Competing Interest

The authors declare no competing financial interest.

#### CRedit authorship contribution statement

**Prinsa R. Nagar:** Methodology, Data curation, Writing – original draft, Writing – review & editing. **Normi D. Gajjar:** Methodology, Data curation, Writing – original draft, Writing – review & editing. **Tejas M. Dhameiya:** Data curation, Conceptualization, Supervision, Writing – original draft, Writing – review & editing.

#### Acknowledgments

A part work of virtual screening mentioned in the present work has been assisted by Drug Discovery Hackathon 2020 (DDH-2020) through the support from Council of Scientific and Industrial Research (CSIR), All India Council of Technical Education (AICTE) and Government of India. Authors would like to acknowledge the support provided by Centre for Development of Advanced Computing (CDAC), Government of India for accessing the virtual tool room for performing molecular modelling.

#### Supplementary materials

Supplementary material associated with this article can be found, in the online version, at doi:10.1016/j.molstruc.2021.131190.

#### References

- [1] M. Nicola, Z. Alsaifi, C. Sohrabi, A. Kerwan, A. Al-Jabir, C. Iosifidis, M. Agha, R. Agha, The socio-economic implications of the coronavirus pandemic (COVID-19): a review, *Int. J. Surg.* 78 (2020) 185–193.
- [2] B. Hu, H. Guo, P. Zhou, Z.L. Shi, Characteristics of SARS-CoV-2 and COVID-19, *Nat. Rev. Microbiol.* 19 (2020) 141–154.
- [3] Q. Li, X. Guan, P. Wu, X. Wang, L. Zhou, Y. Tong, R. Ren, K.S.M. Leung, E.H.Y. Lau, J.Y. Wong, X. Xing, N. Xiang, Y. Wu, C. Li, Q. Chen, D. Li, T. Liu, J. Zhao, M. Liu, W. Tu, C. Chen, L. Jin, R. Yang, Q. Wang, S. Zhou, R. Wang, H. Liu, Y. Luo, Y. Liu, G. Shao, H. Li, Z. Tao, Y. Yang, Z. Deng, B. Liu, Z. Ma, Y. Zhang, G. Shi, T.T.Y. Lam, J.T. Wu, G.F. Gao, B.J. Cowling, B. Yang, G.M. Leung, Z. Feng, Early transmission dynamics in Wuhan, China, of novel coronavirus-infected pneumonia, *N. Engl. J. Med.* 382 (2020) 1199–1207.
- [4] P. Zhou, X. Lou Yang, X.G. Wang, B. Hu, L. Zhang, W. Zhang, H.R. Si, Y. Zhu, B. Li, C.L. Huang, H.D. Chen, J. Chen, Y. Luo, H. Guo, R. Di Jiang, M.Q. Liu, Y. Chen, X.R. Shen, X. Wang, X.S. Zheng, K. Zhao, Q.J. Chen, F. Deng, L.L. Liu, B. Yan, F.X. Zhan, Y.Y. Wang, G.F. Xiao, Z.L. Shi, A pneumonia outbreak associated with a new coronavirus of probable bat origin, *Nature* 579 (2020) 270–273.
- [5] C.C. Lai, T.P. Shih, W.C. Ko, H.J. Tang, P.R. Hsueh, Severe acute respiratory syndrome coronavirus 2 (SARS-CoV-2) and coronavirus disease-2019 (COVID-19): The epidemic and the challenges, *Int. J. Antimicrob. Agents* 55 (2020) 105924.
- [6] L. Wang, Y. Wang, D. Ye, Q. Liu, Review of the 2019 novel coronavirus (SARS-CoV-2) based on current evidence, *Int. J. Antimicrob. Agents* 55 (2020) 105948.
- [7] World Health Organization. Coronavirus disease 2019 (COVID-19). Situation report –51, (2020). [https://www.who.int/docs/default-source/coronavirus/situation-reports/20200311-sitrep-51-covid-19.pdf?sfvrsn=1ba62e57\\_10](https://www.who.int/docs/default-source/coronavirus/situation-reports/20200311-sitrep-51-covid-19.pdf?sfvrsn=1ba62e57_10) (accessed February 2, 2021).
- [8] WHO Coronavirus Disease (COVID-19) Dashboard. <https://covid19.who.int/> (accessed July 12, 2021).
- [9] M.F. Bashir, B. Ma, L. Shahzad, A brief review of socio-economic and environmental impact of COVID-19, *Air Qual. Atmos. Health* 13 (2020) 1403–1409.
- [10] J. Hiscott, M. Alexandridi, M. Muscolini, E. Tassone, E. Palermo, M. Soultioti, A. Zevini, The global impact of the coronavirus pandemic, *Cytokine Growth Factor Rev.* 53 (2020) 1–9.
- [11] S.K.P. Lau, P.C.Y. Woo, K.S.M. Li, Y. Huang, H.W. Tsoi, B.H.L. Wong, S.S.Y. Wong, S.Y. Leung, K.H. Chan, K.Y. Yuen, Severe acute respiratory syndrome coronavirus-like virus in Chinese horseshoe bats, *Proc. Natl. Acad. Sci. U S A.* 102 (2005) 14040–14045.
- [12] S.P. Adhikari, S. Meng, Y.J. Wu, Y.P. Mao, R.X. Ye, Q.Z. Wang, C. Sun, S. Sylvia, S. Rozelle, H. Raat, H. Zhou, Epidemiology, causes, clinical manifestation and diagnosis, prevention and control of coronavirus disease (COVID-19) during the early outbreak period: a scoping review, *Infect. Dis. Poverty* 9 (2020) 29.
- [13] S. Prasad, V. Potdar, S. Cherian, P. Abraham, A. Basu, Transmission electron microscopy imaging of SARS-CoV-2, *Indian, J. Med. Res.* 151 (2020) 241–243.
- [14] Y.Indwiani Astuti, Viral structure and host responses, *Diabetes Metab. Res. Rev.* 14 (2020) 407–412.
- [15] J.F. Drexler, V.M. Corman, C. Drosten, Ecology, evolution and classification of bat coronaviruses in the aftermath of SARS, *Antivir. Res.* 101 (2014) 45–56.
- [16] S.P.K. Pavan Kumar, K. Choudhary, N. Thakur, W. Gaurav Suresh, R. Dayaramani, M. Agrawal, A. Alexander, Virology, pathogenesis, diagnosis and in-line treatment of COVID-19, *Eur. J. Pharmacol.* 883 (2020) 173375.
- [17] K. Mohamed, N. Yazdanpanah, A. Saghadzadeh, N. Rezaei, Computational drug discovery and repurposing for the treatment of COVID-19: a systematic review, *Bioorg. Chem.* 106 (2021) 104490.
- [18] I. de A. Santos, V.R. Grosche, F.R.G. Bergamini, R. Sabino-Silva, A.C.G. Jardim, Antivirals against coronaviruses: candidate drugs for SARS-CoV-2 treatment? *Front. Microbiol.* 11 (2020), doi:10.3389/fmicb.2020.01818.
- [19] N.C. Kyriakidis, A. López-Cortés, E.V. González, A.B. Grimaldos, E.O. Prado, SARS-CoV-2 vaccines strategies: a comprehensive review of phase 3 candidates, *NPJ Vaccines* 6 (2021) 28.
- [20] C. Menni, K. Klaser, A. May, L. Polidori, J. Capdevila, P. Louca, C.H. Sudre, L.H. Nguyen, D.A. Drew, J. Merino, C. Hu, S. Selvaichandran, M. Antonelli, B. Murray, L.S. Canas, E. Molteni, M.S. Graham, M. Modat, A.D. Joshi, M. Mangino, A. Hammers, A.L. Goodman, A.T. Chan, J. Wolf, C.J. Steves, A.M. Valdes, S. Ourselin, T.D. Spector, Vaccine side-effects and SARS-CoV-2 infection after vaccination in users of the COVID symptom study app in the UK: a prospective observational study, *Lancet Infect. Dis.* 21 (2021) 939–949.
- [21] R.T. Eastman, J.S. Roth, K.R. Brimacombe, A. Simeonov, M. Shen, S. Patnaik, M.D. Hall, Remdesivir: a review of its discovery and development leading to emergency use authorization for treatment of COVID-19, *ACS Cent. Sci.* 6 (2020) 672–683.
- [22] M. Martinot, A. Jary, S. Fafi-Kremer, V. Leducq, H. Delagrèverie, M. Garnier, J. Pacanowski, A. Mékinian, F. Pirenne, P. Tiberghien, V. Calvez, C. Humbrecht, A.-G. Marcelin, K. Lacombe, Remdesivir failure with SARS-CoV-2 RNA-dependent RNA-polymerase mutation in a B-cell immunodeficient patient with protracted COVID-19, *Clin. Infect. Dis.* (2020), doi:10.1093/cid/ciaa1474.
- [23] A.S. Rifaoglu, H. Atas, M.J. Martin, R. Cetin-Atalay, V. Atalay, T. Doğan, Recent applications of deep learning and machine intelligence on *in silico* drug discovery: methods, tools and databases, *Brief. Bioinform.* 20 (2019) 1878–1912.

- [24] P.V. Bharatam, Computer-aided drug design, in: R. Poduri (Ed.), *Drug Discovery and Development*, Springer, Singapore, 2021, pp. 137–210.
- [25] P. Shah, T.M. Dhameliya, R. Bansal, M. Nautiyal, D.N. Kommi, P.S. Jadhavar, J.P. Sridevi, P. Yogeewari, D. Sriram, A.K. Chakraborti, *N-Arylalkylbenzo[d]thiazole-2-carboxamides as anti-mycobacterial agents: design, new methods of synthesis and biological evaluation*, *Med. Chem. Commun.* 5 (2014) 1489–1495.
- [26] P.S. Jadhavar, T.M. Dhameliya, M.D. Vaja, D. Kumar, J.P. Sridevi, P. Yogeewari, D. Sriram, A.K. Chakraborti, *Synthesis, biological evaluation and structure-activity relationship of 2-styrylquinazolones as anti-tubercular agents*, *Bioorg. Med. Chem. Lett.* 26 (2016) 2663–2669.
- [27] T.M. Dhameliya, R. Tiwari, A. Banerjee, S. Pancholia, D. Sriram, D. Panda, A.K. Chakraborti, *Benzo[d]thiazole-2-carbanilides as new anti-TB chemotypes: design, synthesis, biological evaluation, and structure-activity relationship*, *Eur. J. Med. Chem.* 155 (2018) 364–380.
- [28] K.A. Bhakhar, N.D. Gajjar, K.B. Bodiwala, D.K. Sureja, T.M. Dhameliya, *Identification of anti-mycobacterial agents against mmpL3: virtual screening, ADMET analysis and MD simulations*, *J. Mol. Struct.* 1244 (2021) 130941.
- [29] N.D. Gajjar, T.M. Dhameliya, G.B. Shah, *In search of RdRp and Mpro inhibitors against SARS CoV-2: molecular docking, molecular dynamic simulations and ADMET analysis*, *J. Mol. Struct.* 1239 (2021) 130488.
- [30] **Protein data bank**. <https://www.rcsb.org/> (accessed August 30, 2020).
- [31] W. Yin, C. Mao, X. Luan, D.D. Shen, Q. Shen, H. Su, X. Wang, F. Zhou, W. Zhao, M. Gao, S. Chang, Y.C. Xie, G. Tian, H.W. Jiang, S.C. Tao, J. Shen, Y. Jiang, H. Jiang, Y. Xu, S. Zhang, Y. Zhang, H.E. Xu, *Structural basis for inhibition of the RNA-dependent RNA polymerase from SARS-CoV-2 by remdesivir*, *Science* 368 (2020) 1499–1504.
- [32] A.J.W. te Velthuis, J.J. Arnold, C.E. Cameron, S.H.E. van den Worm, E.J. Snijder, *The RNA polymerase activity of SARS-coronavirus nsp12 is primer dependent*, *Nucleic Acids Res.* 38 (2010) 203–214.
- [33] D.G. Ahn, J.K. Choi, D.R. Taylor, J.W. Oh, *Biochemical characterization of a recombinant SARS coronavirus nsp12 RNA-dependent RNA polymerase capable of copying viral RNA templates*, *Arch. Virol.* 157 (2012) 2095–2104.
- [34] G.M. Morris, R. Huey, W. Lindstrom, M.F. Sanner, R.K. Belew, D.S. Goodsell, A.J. Olson, *AutoDock4 and AutoDockTools4: automated docking with selective receptor flexibility*, *J. Comput. Chem.* 30 (2009) 2785–2791.
- [35] **Asinex**. <http://www.asinex.com/> (accessed August 17, 2019).
- [36] I.Ahmad Shagufta, *The race to treat COVID-19: potential therapeutic agents for the prevention and treatment of SARS-CoV-2*, *Eur. J. Med. Chem.* 213 (2021) 113157.
- [37] L. Tian, T. Qiang, C. Liang, X. Ren, M. Jia, J. Zhang, J. Li, M. Wan, X. YuWen, H. Li, W. Cao, H. Liu, *RNA-dependent RNA polymerase (RdRp) inhibitors: the current landscape and repurposing for the COVID-19 pandemic*, *Eur. J. Med. Chem.* 213 (2021) 113201.
- [38] Dassault Systèmes BIOVIA, *BIOVIA Workbook, Release 2021; BIOVIA DS Visualizer, Release 2021*, San Diego: Dassault Systèmes, 2021.
- [39] A. Daina, O. Michielin, V. Zoete, *SwissADME: A free web tool to evaluate pharmacokinetics, drug-likeness and medicinal chemistry friendliness of small molecules*, *Sci. Rep.* 7 (2017) 42717.
- [40] **pkCSM: pharmacokinetic properties**. <http://biosig.unimelb.edu.au/pkcsml/prediction> (accessed February 24, 2021).
- [41] D.E.V. Pires, T.L. Blundell, D.B. Ascher, *pkCSM: predicting small-molecule pharmacokinetic and toxicity properties using graph-based signatures*, *J. Med. Chem.* 58 (2015) 4066–4072.
- [42] C.A. Lipinski, F. Lombardo, B.W. Dominy, P.J. Feeney, *Experimental and computational approaches to estimate solubility and permeability in drug discovery and development settings*, *Adv. Drug Deliv. Rev.* 46 (2001) 3–26.
- [43] D.F. Veber, S.R. Johnson, H.Y. Cheng, B.R. Smith, K.W. Ward, K.D. Kopple, *Molecular properties that influence the oral bioavailability of drug candidates*, *J. Med. Chem.* 45 (2002) 2615–2623.
- [44] W.J. Egan, K.M. Merz, J.J. Baldwin, *Prediction of drug absorption using multivariate statistics*, *J. Med. Chem.* 43 (2000) 3867–3877.
- [45] I. Muegge, S.L. Heald, D. Brittelli, *Simple selection criteria for drug-like chemical matter*, *J. Med. Chem.* 44 (2001) 1841–1846.
- [46] A.K. Ghose, V.N. Viswanadhan, J.J. Wendoloski, *A knowledge-based approach in designing combinatorial or medicinal chemistry libraries for drug discovery. I. A qualitative and quantitative characterization of known drug databases*, *J. Comb. Chem.* 1 (1999) 55–68.
- [47] A. Daina, V. Zoete, *A BOILED-Egg to predict gastrointestinal absorption and brain penetration of small molecules*, *ChemMedChem* 11 (2016) 1117–1121.
- [48] J.D. Durrant, J.A. McCammon, *Molecular dynamics simulations and drug discovery*, *BMC Biol.* 9 (2011) 71.
- [49] A. Hospital, J.R. Goñi, M. Orozco, J.L. Gelpí, *Molecular dynamics simulations: advances and applications*, *Adv. Appl. Bioinform. Chem.* 8 (2015) 37–47.
- [50] M. González Torres, E. Villarreal-Ramírez, M. de los A. Moyaho Bernal, M. Álvarez, J. González-Valdez, J.A. Gutiérrez Uribe, G. Leyva Gómez, J.R.C. Cortez, *Insights into the application of polyhydroxyalkanoates derivatives from the combination of experimental and simulation approaches*, *J. Mol. Struct.* 1175 (2019) 536–541.
- [51] T.C. Ramalho, T.C.C. França, W.A. Cortopassi, A.S. Gonçalves, A.W.S. Da Silva, E.F.F. Da Cunha, *Topology and dynamics of the interaction between 5-nitroimidazole radiosensitizers and duplex DNA studied by a combination of docking, molecular dynamic simulations and NMR spectroscopy*, *J. Mol. Struct.* 992 (2011) 65–71.
- [52] S. Abbas, H.H. Nasir, S. Zaib, S. Ali, T. Mahmood, K. Ayub, M.N. Tahir, J. Iqbal, *Carbonic anhydrase inhibition of Schiff base derivative of imino-methyl-naphthalen-2-ol: synthesis, structure elucidation, molecular docking, dynamic simulation and density functional theory calculations*, *J. Mol. Struct.* 1156 (2018) 193–200.
- [53] R.Z. Batran, M.A. Khedr, N.A. Abdel Latif, A.A. Abd El Aty, A.N. Shehata, *Synthesis, homology modeling, molecular docking, dynamics, and antifungal screening of new 4-hydroxycoumarin derivatives as potential chitinase inhibitors*, *J. Mol. Struct.* 1180 (2019) 260–271.
- [54] P. Modi, S. Patel, M. Chhabria, *Structure-based design, synthesis and biological evaluation of a newer series of pyrazolo[1,5-*a*]pyrimidine analogues as potential anti-tubercular agents*, *Bioorg. Chem.* 87 (2019) 240–251.
- [55] V. Hornak, C. Simmerling, *Development of softcore potential functions for overcoming steric barriers in molecular dynamics simulations*, *J. Mol. Graph. Model.* 22 (2004) 405–413.
- [56] M.J. Abraham, Berk Hess, E. Lindahl, D. van der Spoel, *GROMACS 2020.1 (manual version 2020.1)* Zenodo, (2020). 10.5281/zenodo.4054996 (accessed September 10, 2020).
- [57] M.J. Abraham, T. Murtola, R. Schulz, S. Páll, J.C. Smith, B. Hess, E. Lindahl, *GROMACS: high performance molecular simulations through multi-level parallelism from laptops to supercomputers*, *SoftwareX* 1–2 (2015) 19–25.
- [58] O. Trott, A.J. Olson, *Autodock vina: improving the speed and accuracy of docking with a new scoring function, efficient optimization and multithreading*, *J. Comb. Chem.* 31 (2010) 455–461.
- [59] N.M. O’Boyle, M. Banck, C.A. James, C. Morley, T. Vandermeersch, G.R. Hutchison, *Open babel: an open chemical toolbox*, *J. Cheminform.* 3 (2011) 33.
- [60] J. Huang, S. Rauscher, G. Nawrocki, T. Ran, M. Feig, B.L. De Groot, H. Grubmüller, A.D. MacKerell, *CHARMM36m: an improved force field for folded and intrinsically disordered proteins*, *Nat. Methods* 14 (2016) 71–73.
- [61] K. Vanommeslaeghe, E. Hatcher, C. Acharya, S. Kundu, S. Zhong, J. Shim, E. Darian, O. Guvench, P. Lopes, I. Vorobyov, A.D. MacKerell, *CHARMM general force field: a force field for drug-like molecules compatible with the CHARMM all-atom additive biological force fields*, *J. Comput. Chem.* 31 (2010) 671–690.
- [62] W. Yu, X. He, K. Vanommeslaeghe, A.D. MacKerell, *Extension of the CHARMM general force field to sulfonyl-containing compounds and its utility in biomolecular simulations*, *J. Comput. Chem.* 33 (2012) 2451–2468.